TSUNAMI-TIDE INTERACTION IN THE SETO INLAND SEA, JAPAN

Tomohisa Shimoyama[1] and Han Soo Lee[2]

Tsunami-tide interactions in the Seto Inland Sea (SIS) were investigated by taking into account the effects of tidal currents on the tsunami propagation in terms of the arrival time and the run-up heights along the coast of SIS. The initial tsunami wave profile was introduced by the possible Tokai-Tonankai-Nankai Earthquake of the magnitude Mw9.0, which is equivalent to that of 2011 Tohoku Earthquake. Numerical experiments with four different tidal phases, flood, ebb, high, and low, reveal that the water depth changes due to tides affect the tsunami propagation in terms of heights and arrival time. During high tides, the tsunami propagates faster and reaches higher than during the low tides. In addition, during the flood tides with rising water level, tsunami propagates faster than during the ebb tides. Further investigation also shows that the tsunami-tide interaction changes the tsunami signal such that the tsunami-only spectra shifts the spectral peaks after considering the tsunami-tide interactions. Local oscillation modes characterized by local bathymetry and topography shift to higher frequency modes due to the non-linear tsunami-tide interaction. To reduce the uncertainties involved in tsunami predictions and coastal defenses and management, it is strongly recommended to simulate tsunamis together with tides in shallow water environments.

Keywords: Tsunami-Tide interaction; Nankai Trough; the Seto Inland Sea; adaptive mesh refinement

INTRODUCTION

The tsunami on 11 March 2011 induced by the Tohoku Earthquake, Japan, brought an unprecedented and unexpected level of damages. Since then, coastal defenses are required to be revised against possible very large earthquakes, tsunamis and storm surges all over Japan. In the western part of Japan, the potential earthquake and consequential tsunami expected to occur along the Nankai Trough in the next 30 years is a formidable coastal disaster to be considered.

Figure 1 illustrates the revised source rupture and tsunami source area issued in March 2012 by the Central Disaster Prevention Council (Chuo Bousai Kaigi in Japanese; hereinafter CDPC) of the Japanese government. The source rupture and tsunami source area issued in 2003 was largely based on the 1707 Hoei earthquake data. The revised source rupture region in 2012 extended further to the north and west, covering the Shikoku, the Hyuga Nada and the southeastern part of Kyushu. Besides, additional source rupture and tsunami source areas (shaded pink in Fig. 1) south of the Nankai Trough are considered for future disaster prevention for potential very large tsunamis.

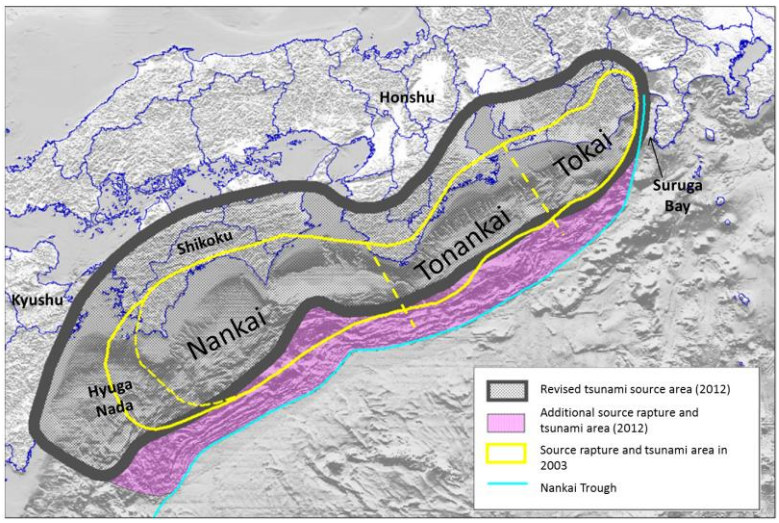

Figure 1. Potential Tokai-Tonankai-Nankai linked earthquake and tsunami source region along the Nankai Trough revised and issued by Central Disaster Prevention Council, Japan, in 2012. (modified from Figure V.3 in the CDPC report for Great Earthquake Model).

[1] Idemitsu Kosan Co. Ltd., Chiba, Japan
[2] Graduate School of Science and Engineering, Saitama University, Shimo-Okubo 255, Sakura-Ku, Saitama-City, Saitama 338-8570, Japan (hslee@mail.saitama-u.ac.jp)

The Seto Inland Sea (SIS) is the largest channel-shaped enclosed coastal sea in the western part of Japan with a size of about 23,000 km^2, a length of about 500 km and an average depth of about 38 m (Lee et al., 2010; Tsuge and Washida, 2003; Yamamoto, 2003; Yanagi et al., 1982). It is connected to the outer Pacific Ocean via the Kii Channel, the Bungo Channel and to the Korea Strait via the Kamon Strait. In addition to its mild climate and beautiful scenery of sandy beaches, tidal flats, and historical heritage, it includes approximately 1000 islands and a number of narrow waterways/straits (Seto in Japanese) connecting the basins (Nada in Japanese) and bays (Fig. 2). Thus, unlike the other coastal regions in Japan, the tide and tidal currents are high and very strong and are important physical processes in the SIS coastal environment. Therefore, it is critical to take the impacts of tides and tidal currents on extreme tsunami propagation in the SIS into account for coastal protection and disaster prevention.

With respect to the tsunami-tide interaction, theoretically, by changing the water depth, tidal elevations influence the speed and magnitude of tsunami waves in shallow regions with dominating tidal signals (Weisz and Winter, 2005). Besides, Kowalik et al. (2006) and Androsov et al. (2010) illustrated through numerical experiments that the non-linear interaction between tide and tsunami in shallow water becomes very significant such that the amplification of tsunami height is mainly associated with strong amplification of tsunami currents, while the linear superposition of sea surface heights from separate tide and tsunami simulations is still valid in deep water. Kowalik and Proshutinsky (2010) also drew a conclusion analogous to previous works through idealized and regional studies that the non-linear tsunami-tide interaction in terms of the tidally-induced water depth and enhanced currents is the main cause for changing the condition of tsunami propagation, amplification and dissipation. In particular, for tsunami run-ups and inundations in coastal, river mouth and estuarine areas, the non-linear interaction of tsunami-tide is critical for an accurate estimation (Kowalik and Proshutinsky, 2010; Zhang et al., 2011).

Therefore, in this study, the impacts of tides and tidal currents on potential extreme tsunami propagation due to the Nankai Trough earthquake were investigated by numerical experiments in the SIS where the tidal ranges are high and the tidal currents are strong.

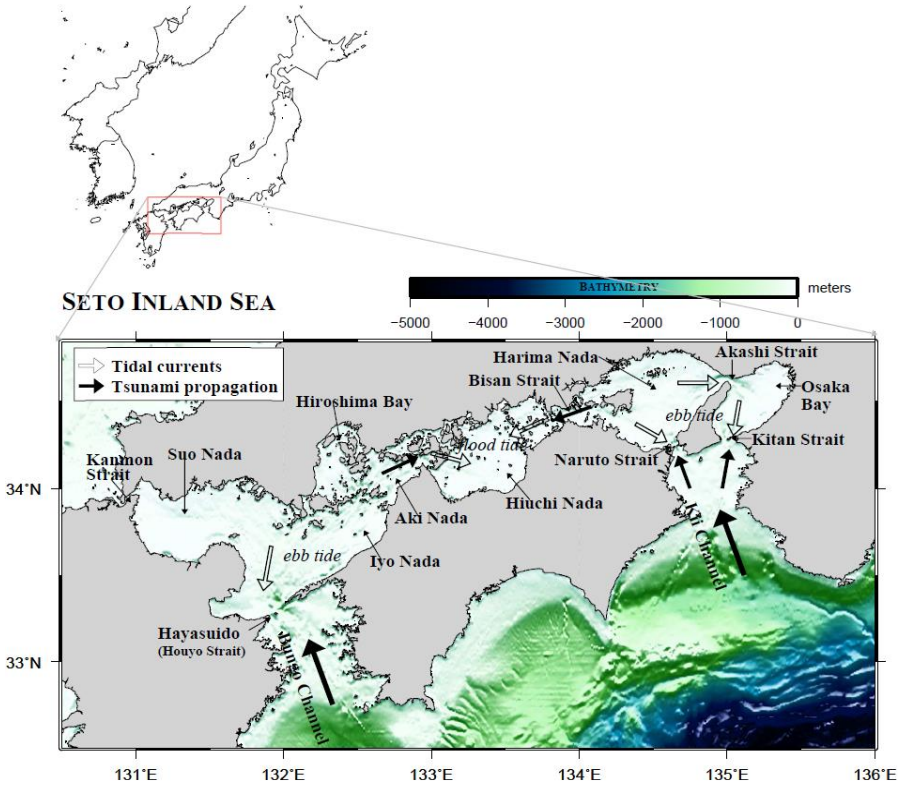

Figure 2. Schematic diagram of potential tsunami-tide interaction in the Seto Inland Sea.

METHOD

Gerris

Gerris is an open source computational fluid dynamic code solving the non-linear shallow water equations. In this section, Gerris is described briefly in terms of the governing equations, the numerical scheme, and the adaptive mesh refinement method. For full details on Gerris and its various applications, please see Popinet (2003; 2011) and Lee et al. (2013).

Governing equations. Tsunamis are most commonly modelled using a long-wave approximation of the mass and momentum conservation equations for a fluid with a free surface. In this approximation, the slopes of both the free surface and the bathymetry are assumed to be vanishingly small. Note that these assumptions are often violated in the case of tsunamis, particularly close to shore, however and somewhat surprisingly, the long-wave approximation still gives reasonable results in practice. Simple scaling arguments show that the vertical velocity of the fluid is also vanishingly small in this context.

Fluid motion can, thus, be described only using the vertically averaged components of the horizontal momentum and the free-surface elevation. The non-linear shallow water equations in conservative form with additional terms for Coriolis Effect and bottom friction can be described as

$$\frac{\partial h}{\partial t}+\frac{\partial}{\partial x}(hu)+\frac{\partial}{\partial y}(hv)=0 \qquad (1)$$

$$\frac{\partial(hu)}{\partial t}+\frac{\partial}{\partial x}\left(hu^2+\frac{1}{2}gh^2\right)+\frac{\partial}{\partial y}(huv)-fv=-hg\frac{\partial z}{\partial x}-c_f|\mathrm{u}|u \qquad (2)$$

$$\frac{\partial(hv)}{\partial t}+\frac{\partial}{\partial x}(huv)+\frac{\partial}{\partial y}\left(hv^2+\frac{1}{2}gh^2\right)+fu=-hg\frac{\partial z}{\partial y}-c_f|\mathrm{u}|v \qquad (3)$$

where h is free surface elevation, $\mathbf{u}=(u, v)$ is the horizontal velocity vector, g is the acceleration due to gravity, z is the depth of bathymetry, f is the Coriolis coefficient, and C_f is the friction coefficient set to 10^{-3} for all numerical experiments.

Adaptivity. Gerris uses a quad tree spatial discretization which allows efficient adaptive mesh refinement. An example of the quad tree structure is exhibited in Fig. 3 together with its logical (tree) representation. This tree can be conveniently described as a "family tree" where each parent cell can have zero or four children cells.

An important parameter is the level of a given cell in the tree. The root cell has level zero by convention and the level increases by one for each successive generation in the tree. A further simplification is obtained by constraining the quad tree so that the level of adjacent cells cannot differ by more than one. This reduces the number of configurations for neighbouring cells to two: (1) neighbouring cells are on the same level: this is identical to a regular Cartesian grid discretization. (2) Two fine cells are neighbouring the same coarse cell (Fig. 3).

In order to refine or coarsen the mesh dynamically, it is necessary to choose a refinement criterion. This choice is not trivial and depends on both the details of the numerical scheme which control how discretization errors and the physics of the problem considered which control how discretization errors will influence the accuracy of the solution. Gerris provides a variety of refinement criteria which can be flexibly combined depending on the problem. In this study, the gradient of free surface elevation was used for the refinement criterion. Cells also need to be coarsened when a high spatial resolution is not required anymore. When cells are coarsened, the values of fields are set by defaults to the averages over their children, which also ensure conservation of quantities.

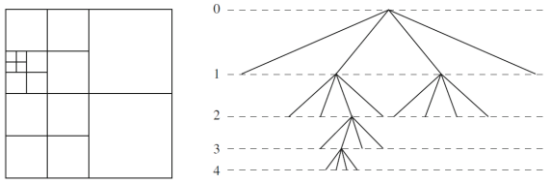

Figure 3. Example of quad tree discretization (left) and its local representation together with the level of the cells in the tree (right).

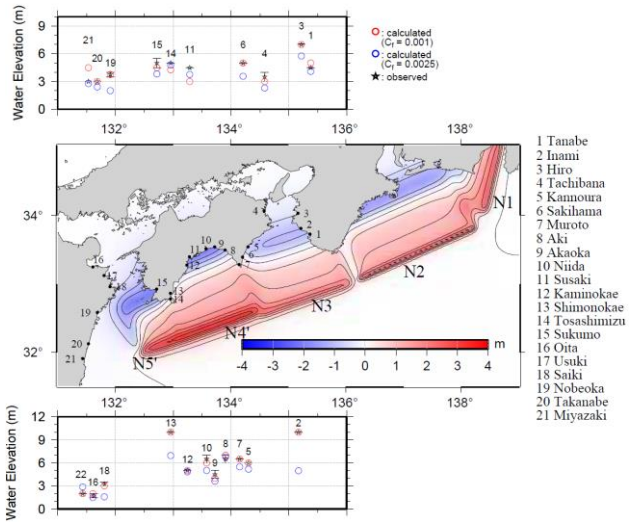

Figure 4. Comparisons between the observed tsunami run-up heights and the calculated maximum tsunami heights along the Pacific coast of Japan for the 1707 Hoei Earthquake tsunami.

Table 1. Numerical experiments scenarios

Run	Tidal phase	Tidal boundary	Remarks
TSUNAMI	×	×	•Based on the tidal phase at Hayasuido
HIGH	High	M_2, S_2, K_1 and O_1	•Spin-up: approx. 2 days
EBB	Ebb		•Simulation period: 10 hr
LOW	Low		•Initial water displacement: Case 1 from NDPC report
FLOOD	Flood		

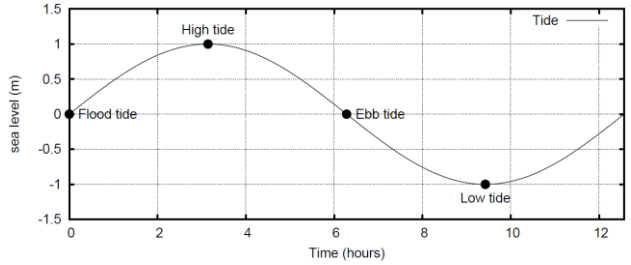

Figure 5. Definitions of four different tidal phases considered in the numerical experiments. Tidal phase at Hayasuido is considered for baseline in the experiments.

Validations of Gerris

Tides in the Seto Inland Sea. The M_2 tide in the SIS was modeled with Gerris for its validation. A numerical simulation was carried out with only M_2 tidal open boundary. For the coastline/land boundary, the rigid and impermeable boundary condition is applied to flow motion which is expressed in the numerical model by a zero normal flow. Open tidal boundary conditions were imposed from the global ocean tide model, FES2004 (Lyard et al., 2006). The FES2004 is a combined product based on a hydrodynamic model which assimilates tide gauges and altimeter data from Topex/Poseidon and ERS-2 on a 1/8 ° × 1/8 ° grid. The bathymetry data for experiments is taken from the GEBCO 30 arc-sec database (IOC et al., 2003), which is referenced with respect to mean sea levels. The simulation period for the M_2 tide was 7 days. Compared with previous studies (Kobayashi et al., 2006; Yanagi and Higuchi, 1981) in terms of co-amplitude, co-phase, and tidal ellipse charts of M_2 tide, the characteristics of simulated M_2 tide such as tidal amplitudes and phases in the SIS described above are

well agreed with (not shown here). The Suo Nada and the Hiuchi Nada appears to have in almost the same tidal phase indicating of the rising and falling of water levels like standing waves within each nada, respectively.

The 1707 Hoei Earthquake Tsunami. The historical 1707 Hoei Earthquake tsunami was also modeled for its validation. Figure 4 illustrates the 1707 Hoei Earthquake tsunami source region (middle panel) based on the revised faults parameters proposed by Furumura et al. (2011). The 1707 Hoei Earthquake tsunami simulations were carried out with varying friction coefficients and the simulation result with friction coefficient of 0.001 showed the best performance compared with the historical tsunami records (the top and bottom panels in Fig. 4). The simulation result with different friction coefficient can also be found in the figure. The historical tsunami records are obtained from Hatori (1974; 1985) and Murakami et al. (1996). The same bathymetry from GEBCO 30 arc-sec was also used for the tsunami simulation.

Numerical experiments

Numerical experiments based on the scenarios in Table 1 were conducted to investigate the impacts of tidal currents on tsunami propagation in the SIS. The 4 tidal phases defined (Fig. 5) and considered in the experiments are based on those at Hayasuido, because the tidal current at Hayasuido is one of the fastest currents in the SIS.

For the tidal open boundary, the 4 major constituents M_2, S_2, K_1 and O_1 are imposed from the same FES2004 global tide model. The same GEBCO bathymetry is used for the experiments. The variable resolution is also applied to implement "sponge layers" on the open boundaries of the domain. Along all boundaries of the domain, the spatial resolution is coarsened to 5 levels. Therefore, the resulting numerical dissipation dampens waves before they exit the domain, thus minimizing spurious tsunami wave reflections at boundaries.

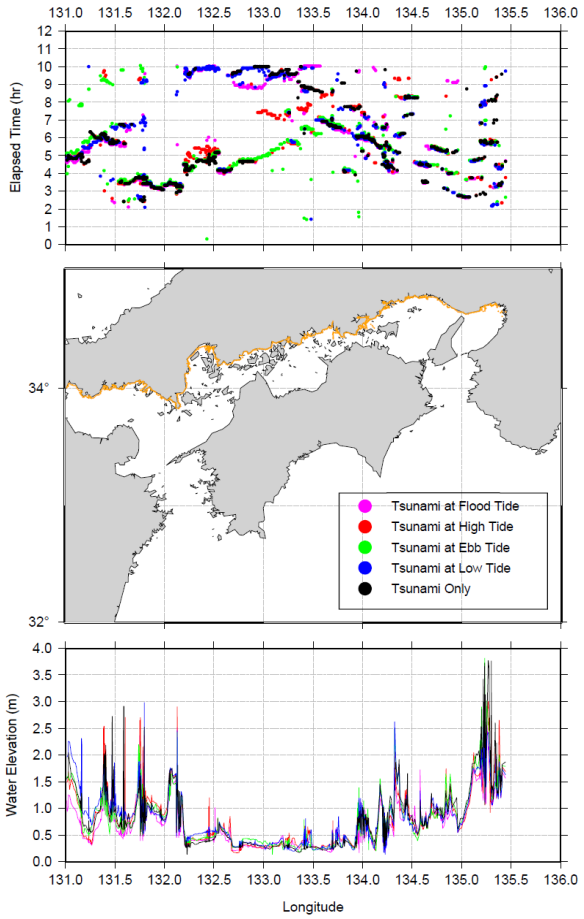

Figure 6. Calculated maximum tsunami heights (bottom) and their arrival times (top) along the Honshu coast of the SIS (middle) from numerical experiments. Each color indicates the different experiments at respective tidal phases.

RESULTS

Figure 6 shows the calculated maximum tsunami heights and their arrival times at probes along the Shikoku coast from the five experiments. In the bottom panel of the figure, the legend, Tsunami, indicates the result from the tsunami-only case, while the others, such as at Flood, at High, at Ebb, and at Low, represent the tsunami heights in time obtained by the difference between the joint tsunami-tide simulations and the tide-only simulation. Note that the baseline of tidal phases is those at Hayasuido. The SIS is divided into 6 sections, such as the Bungo Channel (BC), the Suo Nada and the Iyo Nada (SI), the Hiroshima Bay and the Aki Nada (HA), the Hiuchi Nada (HN), the Harima Nada and the Osaka Bay (HO), and the Kii Channel (KC). Their results are described in the following.

The maximum tsunami heights with tide interaction at all probes in the Bungo Channel are almost the same compared to the tsunami height from the tsunami alone case. However, the tsunami heights of the first waves at Uwajimasi are reduced more compared to other probes. The maximum tsunami heights from joint tsunami-tide simulations at Uwajimasi appear between 5 and 6 hrs in elapsed time and are amplified due to non-linear tsunami-tide interactions.

In the Suo Nada and the Iyo Nada, the maximum tsunami heights from joint simulations are increased or decreased at probes. The tsunami heights of the first waves are all increased in joint simulations. The arrival times of the first peaks depending on tidal phase are slightly earlier than those of the tsunami alone case. At Simonoseki-Oki and Toyomaesi, the tsunami heights of the first peaks are enhanced or reduced considerably depending on tidal phase compared to those without the influence of tides. The first peaks at Shimonoseki-Oki and Toyomaesi arrive approximately 30-min earlier than those of the tsunami alone case.

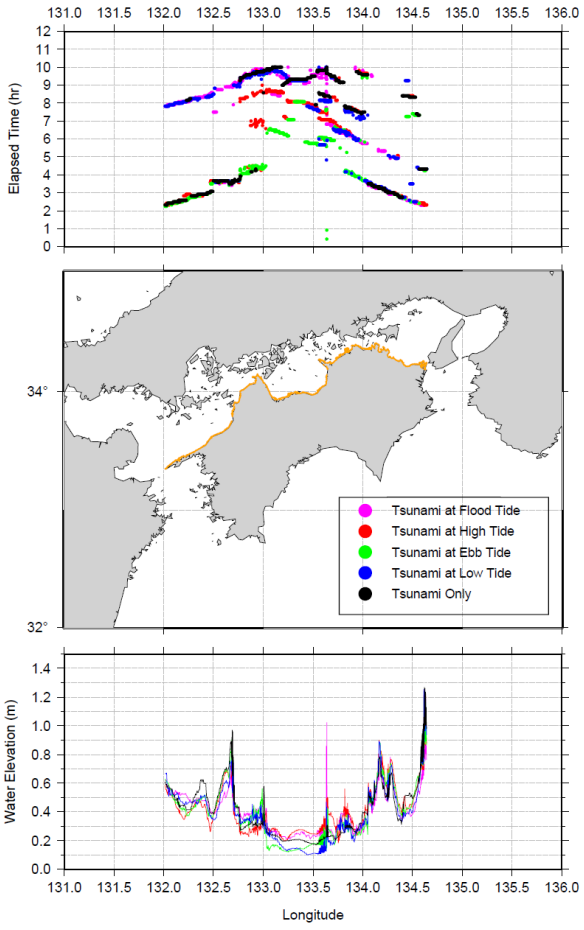

Figure 7. Calculated maximum tsunami heights (bottom) and their arrival times (top) along the Shikoku coast of the SIS (middle) from numerical experiments. Each color indicates the different experiments at respective tidal phases.

The calculated tsunami heights in the Hiroshima Bay and the Aki Nada exhibit a similar tendency. The maximum tsunami heights with tidal interactions are enhanced or reduced, and the impacts of tides are clearly seen in the arrival times of the first waves.

In the Hiuchi Nada, the center of the SIS, the maximum tsunami heights calculated with tide interactions are reduced compared the tsunami alone case. The sea level variations for the beginning 4 hours are the oscillation due to the negative initial displacement of surface and the tsunami waves due to the positive displacement from the outer SIS arrive into the Hiuchi Nada after about 4 hours.

In the Harima Nada and the Osaka Bay, the tendency in the maximum tsunami heights and the arrival times of the first waves calculated with tide interactions are similar with those in other nadas and bays, showing enhancement or reduction depending on tidal phase. The probes in the Harima Nada show relatively large differences in the maximum tsunami heights with and without tide interaction, while the Osaka-Oki in the Osaka Bay shows slight change in the maximum tsunami height. The temporal variations of tsunami heights in the Harima Nada and the Osaka Bay are different significantly place by place.

At the probes in the Kii Channel such as Wakayama-Oki, Aritasi, and Tanabe, the overall results illustrated are similar to those at the Bungo Channel. The maximum tsunami heights with tide interactions become larger than those from the tsunami only case, and the arrival times of the first waves are more or less the same as for the tsunami only case since the probes are located close to the positive tsunami source area.

Along the Honshu coast in the SIS in Fig. 6, the maximum tsunami heights in Suo Nada show large differences depending on the tidal phases, while in the other nadas the differences are not that large. With respect to the arrival times, each basin illustrates its characteristics very well. In Suo Nada, the reflected waves play important roles producing the maximum tsunami heights. In Osaka-Bay and Harima Nada, the bay-scale oscillations affect the maximum tsunami heights. In the calculated maximum tsunami heights along the Shikoku coast in Fig. 7, the large differences can be found in the heights and arrival times. The bay-scale oscillation also plays an important role that the maximum tsunami heights appear in periodically.

TSUNAMI-TIDE INTERACTIONS

The SIS is unique in terms of tidal environment as the tide enters the sea in the two channels and meets near the Hiuchi Nada, the center of the SIS. There is an approximately 5- to 6-hr difference in the tidal phase between the entrance of the channels and the Hiuchi Nada. Figure 8 present the calculated sea level variations from the numerical experiments at Hayasuido in Bungo Channel, at Shimonoseki-Oki in the inner part of the SIS, and at Fukuyama-Oki in the center of the SIS, respectively. Each panel exhibits the sea level variations caused by the tide-only, the tsunami-only, the joint tsunami-tide, and the difference between the joint tsunami-tide and the tide-only.

The results at Shimonoski-Oki in Fig. 8 show the effects of tides clearly. The tidal range is nearly 5 m at the probe. The first peaks of the tsunami waves appear at Flood, at Low, at High, and at Ebb phase in order, which are at high, at flood, at ebb and at low tides in local phase. The order of the tsunami heights of the first peaks is at Flood, at Low, at Ebb, and at High phase, which are at high, at flood, at low and at ebb tides in its local tidal phase. In terms of the water depth change, the results at high and low tides depict its influence clearly in the propagation speeds as well as the heights of tsunami waves such that the tsunami at high tide appears earlier and higher than at low tide. With respect to the tidal currents, the results at flood and ebb tides also illustrate its effect clearly on the tsunami propagations. The tidal currents at flood and ebb are the strongest and those at high and low are zero. At Shimonoseki-Oki in the inner part of the SIS, the tidal currents are fast with strong directionality at flood and ebb tides. It means that the tidal currents at flood are inward currents at Shimonoseki-Oki in the Suo Nada which is the same as the inwards tsunami propagation, while those at ebb are outward currents which is the opposite direction compared to tsunami propagation. Therefore, it can be deduced that the tidal current enhances the tsunami propagation at Shimonoseki-Oki during flood tides resulting in faster tsunami propagation and higher tsunami height.

Those effects of tides on tsunamis through the non-linear interactions are found at other probes analogously. In the results, it can be seen that the larger tidal range at a probe, the more distinct influence of tides in tsunami propagations. In terms of tidal currents, it illustrates that the arrival times of the first waves during the inward flood tide in the SIS are earlier than those at ebb tide.

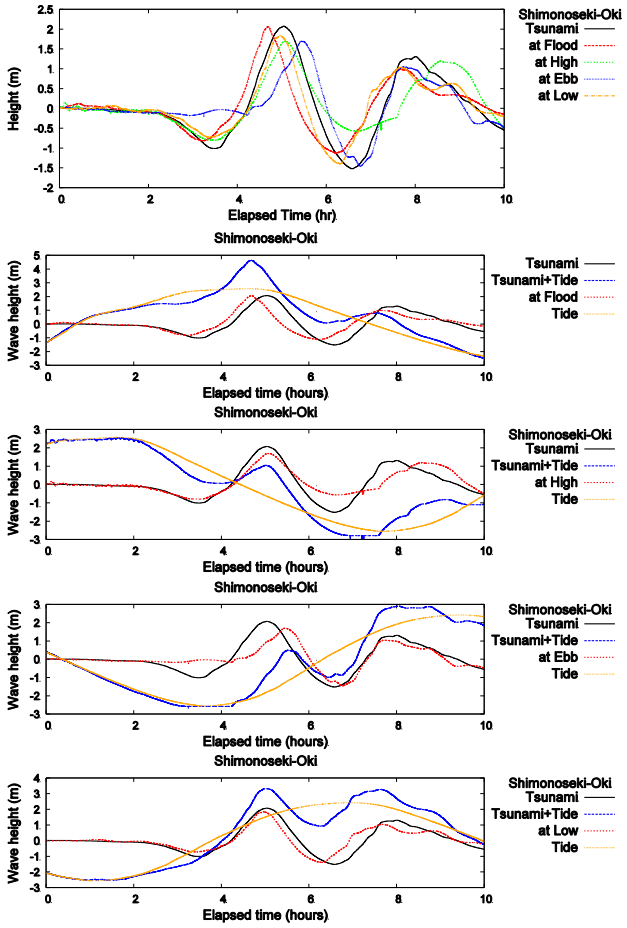

Figure 8. Comparisons of calculated tsunami heights at 4 tidal phases with tide only results (the top panel). Each panel from the second to the bottom presents the sea level variations from the tsunami-only (Tsunami), the joint tsunami-tide simulations (Tsunami+Tide), the tsunami heights (at Phase) obtained by (Tsunami+Tide)-(Tide), and the tide-only (Tide).

Tsunami spectra for coastal areas are known to be similar for different events at the same station and dissimilar for the same event for different stations affected by local topography and bathymetry, such as by the continental shelves and associated bays and harbors (K Abe, 1990; T Abe, 1984; Rabinovich, 1997). To investigate further on the non-linear tsunami-tide interaction, we conducted additional tsunami-only simulations for all 11 tsunami scenarios proposed by the CDCP. Configurations of the model for additional tsunami-only simulations is the same for the tsunami-only experiment as described in Section 2.

Figure 9 illustrates the spectral densities of tsunami heights from the joint tsunami-tide simulation and the 11 tsunami-only cases at Hayasuido. In the 11 tsunami-only results, we obtain the density peaks at the same frequencies even though energy levels are slightly different case by case, which confirms the previous statement that tsunami spectra for coastal areas are known to be similar for different events at the same location. However, the same peaks are not appeared in the joint tsunami-tide results. For instance, the peaks at the period of 45 min in the tsunami-only cases do not appear in the joint tsunami-tide results. Then, new resonance modes with shorter period of approximately 31 min appear in the joint tsunami-tide simulations due to the non-linear tsunami-tide interaction.

CONCLUSIONS

This paper investigates the impacts of tides and tidal currents on tsunami propagation in the Seto Inland Sea, Japan, based on numerical experiments. Tsunami experiments are conducted based on five scenarios taking the tides and tidal currents at 4 different phases, such as flood, high, ebb, and low tides, into account. The initial tsunami displacement is adopted from the first case scenario announced in the first report of the CDPC in Japan for the potential extreme tsunami due to the Tokai-Tonankai-Nankai

linked earthquake along the Nankai Trough. The numerical experiments are conducted using an open-source non-linear shallow water equation model with adaptive mesh refinement method.

Based on the results of numerical experiments, the general effects of changed water depth due to tides on tsunami propagation are confirmed such that higher tsunami heights and earlier tsunami arrival at high tide are obtained compared to those at low. The maximum tsunami heights at probes in and out of the SIS are enhanced or reduced after considering the non-linear tsunami-tide interaction. In terms of the effects of tidal currents on tsunami propagation, it is shown that the strong inward tidal currents at flood tide result in higher and faster tsunami propagation in the SIS, whereas the opposing outward tidal currents to tsunami propagation at ebb tide result in lower tsunami heights and slower arrival time. The probes in the Bungo and Kii Channel show less significant effects of tides and tidal currents on tsunami propagation. However, the probes in the SIS where the tidal ranges are relatively large compared to those out of the sea depict large differences in the maximum tsunami heights and in the arrival times of the first waves. For example, the differences of the maximum tsunami height and the arrival time of the first peaks at Shimonoseki-Oki and Toyomaesi depict 0.37 m and 0.52 m and nearly 1 hr among the joint tsunami-tide results.

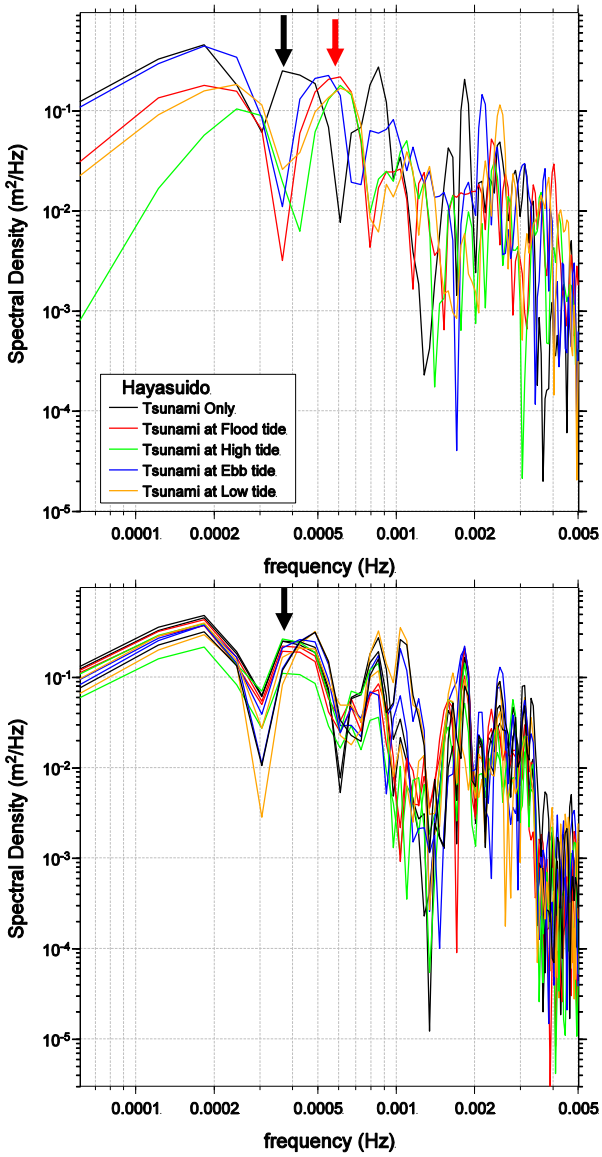

Figure 9. Spectral density plots for the calculated tsunami heights at Hayasuido from the tsunami-tide joint simulations (top) and from the 11 tsunami-only simulations (bottom) proposed by the CDCP report.

Based on the power spectrum analysis, it is shown that the non-linear tsunami-tide interaction creates new oscillation modes in higher frequency which do not appear in the tsunami-only simulations. The non-linear tsunami-tide interaction may enrich the tsunami height signals, resulting in the new oscillation modes in higher frequencies than the approximated tsunami frequencies and the local oscillation modes of bays and harbors.

The main conclusion of this study is that tsunami-tide interactions have a wide range of impacts on tsunami propagation in the SIS where the tides and tidal currents are high and strong in this shallow water environment, depending also on the individual basin and bay bathymetry and coastline configuration. In general, the non-linear interaction of tsunami and tide in the near-shore region can enhance or reduce the total sea level and currents. Therefore, to reduce the uncertainties involved in tsunami predictions and coastal defenses and management, it is strongly recommended to simulate tsunamis together with tides in shallow water environments. However, the uncertainty coming from the water depth changes due to initial bottom deformation by fault motions are not considered in all experiments of this study.

Finally, this study illustrates the importance of physical interaction between extreme tsunamis and tides and tidal currents in tsunami propagation in the high tide range and strong tidal current environments including the SIS, Japan. Moreover, the study intends to supplement the CDPC report in this manner, and neither to compare nor to replace the results of the CDPC report. Note also that the locations and names of probes in the SIS in this study are arbitrarily decided by the authors, and they are not the same as those in the CDPC reports.

ACKNOWLEDGMENTS

The views expressed herein are those of the authors and do not reflect the views of their institutions. This research is supported by the Grant-in-Aid for Young Scientists B (24760396) and by the Grant-in-Aid for Challenging Exploratory Research of the Ministry of Education, Culture, Sports, Science, and Technology (MEXT), Japan. It is also supported by the Research Fund (23117) of the Kurita Water and Environment Foundation (KWEF).

REFERENCES

Abe, K. 1990. Spectral Characteristics of the 1983 Japan Sea Tsunami Observed in Japan, *The science reports of the Tohoku University. Fifth series, Tohoku geophysical journal*, *33*(2), 97-106.

Abe, T. 1984. Baywater response to tsunamis, *Proceedings of 19th International Conference on Coastal Engineering*, Houston, Texas.

Androsov, A., J. Behrens, and S. Danilov. 2010. Interaction between tides and tsunami waves, *Proc. of the Indian Ocean Tsunami Modelling Symposium*, Fremantle, Western Australia.

Furumura, T., K. Imai, and T. Maeda. 2011. A revised tsunami source model for the 1707 Hoei earthquake and simulation of tsunami inundation of Ryujin Lake, Kyushu, Japan, *Journal of Geophysical Research: Solid Earth*, *116*(B2), B02308.

Hatori, T. 1974. Sources of large tsunamis in southwest Japan (in Japanese), *J. Seismol. Soc. Jpn.*, *27*, 10-24.

Hatori, T. 1985. Field investigation of historical tsunamis along the east coast of Kyushu, West Japan (in Japanese), *Bull. Earthquake Res. Inst. Univ. Tokyo*, *60*, 439-459.

IOC, IHO, and BODC. 2003. Centenary Edition of the GEBCO Digital Atlas, published on CD-ROM on behalf of the Intergovernmental Oceanographic Commission and the International Hydrographic Organization as part of the General Bathymetric Chart of the Oceans.

Kobayashi, S., J. H. Simpson, T. Fujiwara, and K. J. Horsburgh. 2006. Tidal stirring and its impact on water column stability and property distributions in a semi-enclosed shelf sea (Seto Inland Sea, Japan), *Continental Shelf Research*, *26*(11), 1295-1306.

Kowalik, Z., and A. Proshutinsky. 2010. Tsunami–tide interactions: A Cook Inlet case study, *Continental Shelf Research*, *30*(6), 633-642.

Kowalik, Z., T. Proshutinsky, and A. Proshutinsky. 2006. Tide-Tsunami interactions, *Science of Tsunami Hazards*, *24*(4), 242-256.

Lee, H. S., T. Yamashita, T. Komaguchi, and T. Mishita. 2010. Storm surge in Seto Inland Sea with Consideration of the Impacts of Wave Breaking on Surface Currents, *Proceedings of the 32nd International Conference on Coastal Engineering*, ASCE, Shanghai.

Lee, H. S., T. Komaguchi, A. Yamamoto, and M. Hara. 2013. Wintertime Extreme Storm Waves in the East Sea: Estimation of Extreme Storm Waves and Wave-Structure Interaction Study in the Fushiki Port, Toyama Bay, *Journal of Korean Society of Coastal and Ocean Engineers*, *25*(5), 335-347.

Lyard, F., F. Lefevre, T. Letellier, and O. Francis. 2006. Modelling the global ocean tides: modern insights from FES2004, *Ocean Dynamics*, *56*(5-6), 394-415.

Murakami, H., T. Shimada, S. Itoh, N. Yamamoto, and J. Ishizuka. 1996. Reexamination of the heights of the 1605, 1707 and 1854 Nankai Tsunamis along the coast of Shikoku Island (in Japanese), *J. Jpn. Soc. Nat. Disaster Sci.*, *15*(1), 39-52.

Popinet, S. 2003. Gerris: a tree-based adaptive solver for the incompressible Euler equations in complex geometries, *Journal of Computational Physics*, *190*(2), 572-600.

Popinet, S. 2011. Quadtree-adaptive tsunami modelling, *Ocean Dynamics*, *61*(9), 1261-1285.

Rabinovich, A. B. 1997. Spectral analysis of tsunami waves: Separation of source and topography effects, *Journal of Geophysical Research: Oceans*, *102*(C6), 12663-12676.

Tsuge, T., and T. Washida. 2003. Economic valuation of the Seto Inland Sea by using an Internet CV survey, *Marine Pollution Bulletin*, *47*(1-6), 230-236.

Weisz, R., and C. Winter. 2005. Tsunami, tides and run-up: a numerical study, *Proc. of the International Tsunami Symposium*, Chania, Greece.

Yamamoto, T. 2003. The Seto Inland Sea--eutrophic or oligotrophic?, *Marine Pollution Bulletin*, *47*(1-6), 37-42.

Yanagi, T., and H. Higuchi. 1981. Tides and tidal currents in the Seto Inland Sea (in Japanese), *Proc. 28th Conf. on Coastal Engineering, Japan Soc. Civil Eng.*, 555-559.

Yanagi, T., H. Takeoka, and H. Tsukamoto. 1982. Tidal energy balance in the Seto Inland Sea, *Journal of Oceanography*, *38*(5), 293-299.

Zhang, Y. J., R. C. Witter, and G. R. Priest. 2011. Tsunami–tide interaction in 1964 Prince William Sound tsunami, *Ocean Modelling*, *40*(3–4), 246-259.